Members of the LLNL x-ray holography team: (l. to r.) Steve Brown, Jim Trebes, Dave Nilsson, and Dennis Matthews. This photograph was taken in the fall of 1989 as they prepared for second generation x-ray holography experiment. The Nova laser's two-beam target chamber is in the background.

Research Applications

X-ray optics have matured sufficiently to permit the development and research application of x-ray laser cavities, x-ray microscopy, and x-ray holography.

In just the past few years, the emerging field of x-ray optics has reached a new stage of maturity. All the basic optical components that are typically taken for granted at visible wavelengths are now available, as well as high-brightness, (partially) coherent x-ray sources, and advanced detection systems for both real-time and ultrafast imaging.

These components are now beginning to be integrated into sophisticated optical systems at soft-x-ray wavelengths, both at LLNL and elsewhere. Active research programs are under way to develop cavities for x-ray lasers as well as x-ray microscopes and holographic systems for high-resolution imaging of living microorganisms. Here we review these relatively mature activities.

X-Ray Laser Cavities

An early motivation for the development of normal-incidence mirrors and beamsplitters at LLNL was the need for resonant cavities for the newly developed soft-x-ray sources of ASE. Cavity development is a crucial step in the transformation of these x-ray gain media into efficient x-ray lasers with optimized divergence and coherence properties.

The fundamental problems in the development of x-ray laser cavities are optics survival, radiation transport, and short gain lifetime. Typical soft-x-ray gain media are short-duration, high-temperature, high-density plasmas that have been produced by intense optical-laser irradiation of foil, fiber, or solid targets. These gain media are a hostile environment for multilayer cavity optics, and the short gain lifetime leaves little opportunity for many amplification passes. In addition, the gain medium itself may be subject to local inhomogeneities that could compromise the coherent transport of amplified radiation.

At LLNL, we have made significant progress in overcoming these challenges. Experiments demonstrating the survival of molybdenum/silicon multilayer mirrors in the hostile x-ray laser environment have been completed, and results are in agreement with calculations of mirror damage thresholds.

We have also performed several series of double-pass and triple-pass cavity demonstration experiments on neon-like collisional excitation laser systems. An important feature of these experiments was the 20-ps time resolution of cavity output. This permitted temporal separation and distinct identification of the single-, double-, and triple-pass amplified beams.

This detailed monitoring of the amplification process in these experiments enabled us to:

- Demonstrate the viability of multipass cavity optics.

• Unequivocally demonstrate and measure the double-pass/single-pass amplification ratio.
• Demonstrate the viability of double-pass cavities at wavelengths as short as 13.1 nm.
• Unfold the "effective" gain-length product at 20.63 and 20.96 nm in the neon-like selenium laser.

The typical output from a single-pass, neon-like x-ray laser is a single pulse in time with a duration of about 170 ps (FWHM). Careful selection of cavity parameters in a double-pass experiment will allow the output stimulated by the reflected beam to be separated in time from the initial pulse. Cavity output data at 20.96 and 20.63 nm from two such experiments are presented in Figure 17. In these experiments, the cavity mirrors were flat molybdenum/silicon multilayers placed 3.0 cm from the end of the gain medium in 17a and 3.5 cm from the end in 17b. The measured normal-incidence reflectivity of the mirrors was 15% and 26% in 17a and 17b, respectively.

In the first experiment (17a), the double-pass signal was approximately an order of magnitude more intense than the single-pass ASE. The best double-pass/single-pass intensity enhancement achieved in this experimental series was ~20×, with a radiant intensity (W/sr) increase of ~600× (due to an ~6× decrease in divergence).

The data from the second experiment (17b) provide a clearer delineation of the single- and double-pass beams in a double-pass experiment. They show a peak-to-peak separation of the signals of ~300 ps, consistent with the path difference of 9 cm between the single- and double-pass beams. Also, the double-pass signal lasts longer than the single-pass signal (210 vs 170 ps FWHM).

A demonstration of double-pass amplification in neon-like molybdenum at 13.27 and 13.1 nm is shown in Figure 18. This is the shortest wavelength cavity demonstration to date. In this experiment, the cavity mirror was a flat molybdenum/silicon multilayer placed 2.5 cm from the end of the gain medium. Its measured normal-incidence reflectivity is precisely that shown already in Figure 7c. Figure 18 also shows the laser line emission at 13.94 nm. This line has lower gain than the others and is outside the bandpass of the mirror. As a result, its intensity is lower and it does not have a double-peaked time distribution.

The most sophisticated demonstration to date of soft-x-ray

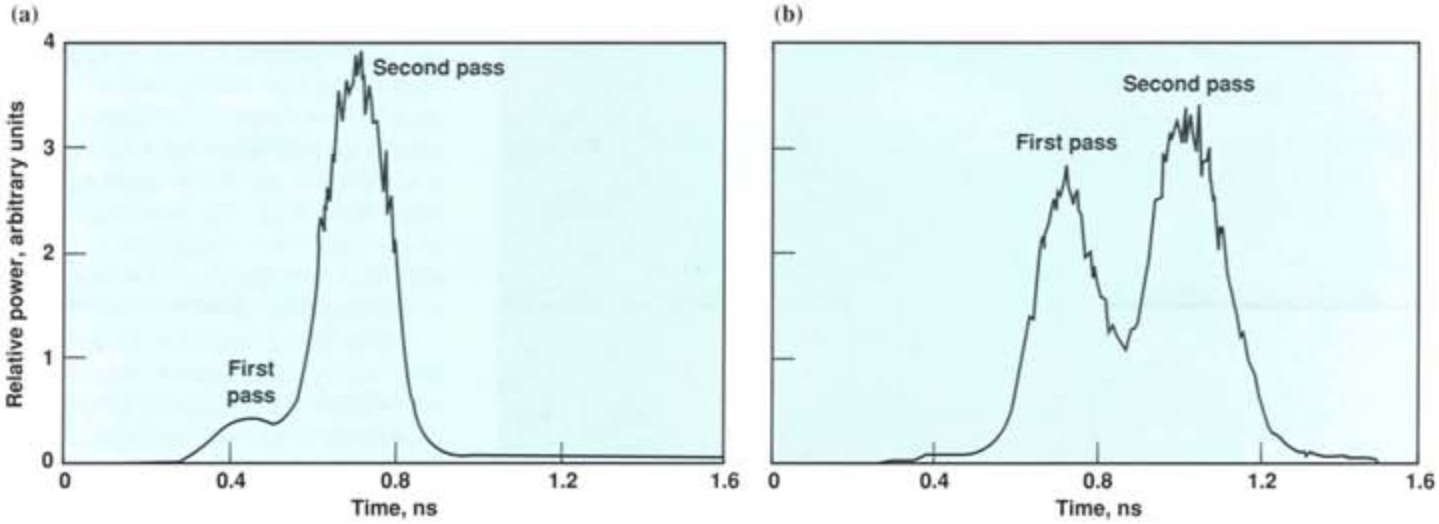

Figure 17. Multilayer mirror cavities are being used to enhance the output power and analyze the time-varying gain of laboratory x-ray lasers. Double-pass cavity output data for two different x-ray laser experiments are presented. The cavity was designed to allow distinct identification of the (early) single-pass and (later) double-pass amplified beams. In experiment (a), the double-pass beam is an order of magnitude more powerful than the single-pass beam. In experiment (b), the two beams have roughly equal power.

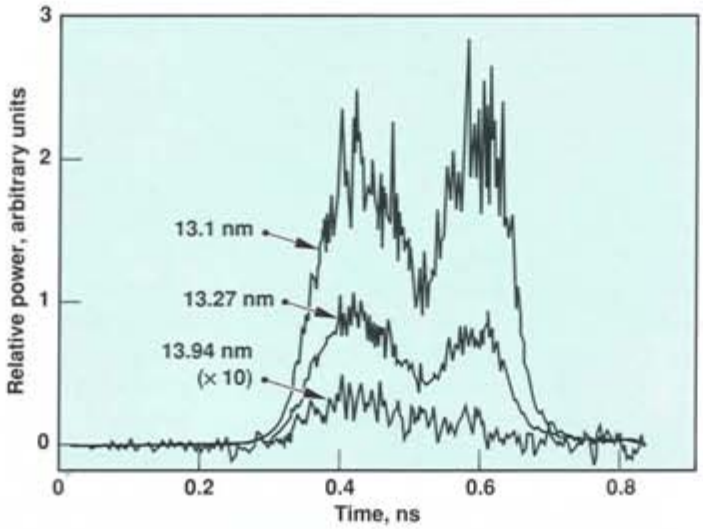

Figure 18. Results from a double-pass cavity experiment in neon-like molybdenum, showing amplification at 13.27 and 13.1 nm but no amplification on the 13.94-nm line, which is outside the bandpass of the cavity mirror.

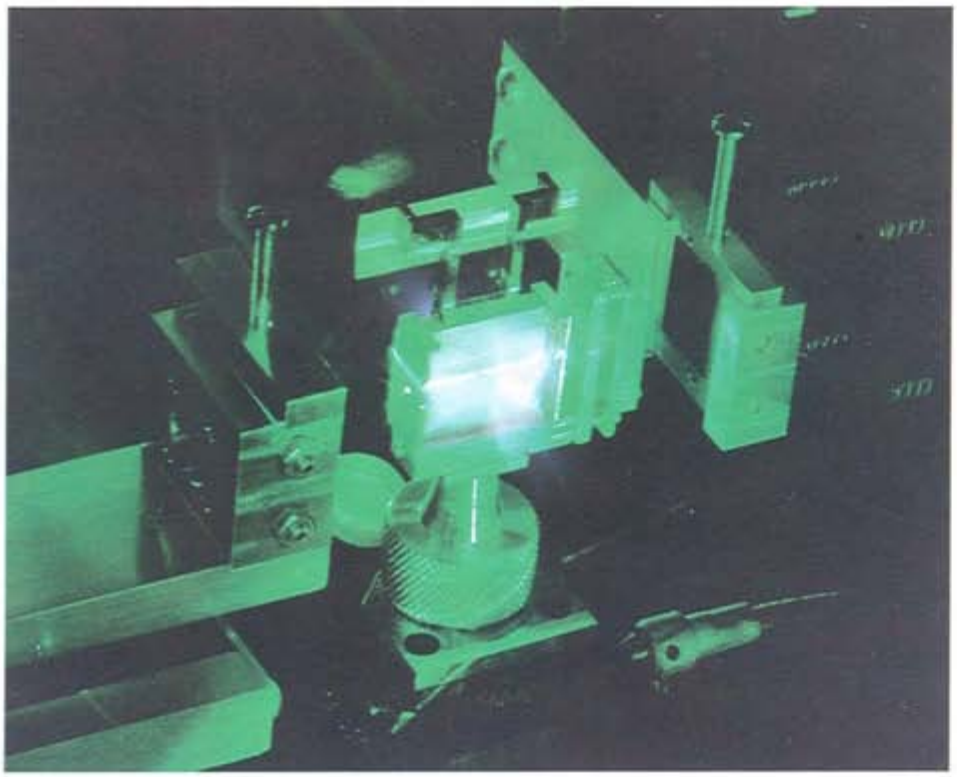

Figure 19. Multipass x-ray laser cavity apparatus in operation at LLNL. In the summer of 1987, the first demonstration of multipass amplification of soft x rays was performed on the Nova two-beam target facility at LLNL. These experiments grew out of a collaboration between the Laboratory's x-ray laser group (Dennis Matthew and colleagues) and advanced x-ray optics group (Nat Ceglio and colleagues). At the center of the photograph is the exploding-foil, neon-like selenium x-ray laser. At the left is the holder for the cavity multilayer mirror; at the right is the multilayer beamsplitter. X radiation bounces back and forth inside the cavity, being further amplified on each pass through the exploding-foil region. Radiation output is achieved by the partial transmission of the beamsplitter. Output data are shown in Figure 20.

laser cavity performance is illustrated in Figures 19 and 20. Figure 19 shows the cavity optics along with the exploding foil selenium laser. Figure 20 shows the time-resolved triple-pass amplified output (at 20.63 nm) from this multipass cavity. In the experiment, the cavity consisted of a spherical mirror (12-cm radius) placed 3.5 cm from one end of the gain medium and a flat beamsplitter placed 3.0 cm from the other end. The gain medium was a neon-like selenium plasma 2 cm long. The cavity mirror was a molybdenum/silicon multilayer (d = 11.1 nm, $\gamma = 0.4$, $N = 30$) deposited on a highly polished BK-7 substrate. Its measured reflectivity at 20.63 nm was ~20%. The beamsplitter was a molybdenum/silicon multilayer (d = 11.4 nm, $\gamma = 0.5$, $N = 6$) supported by a 40-nm-thick silicon nitride membrane. Measured beamsplitter reflectivity and transmission at 20.63 nm were 15 and 5%, respectively. The single-, double-, and triple-pass amplified signals are easily identified in Figure 20. The double-pass signal is 22 times more intense and the triple-pass signal is about the same intensity as the single-pass ASE. The low intensity of the triple-pass signal is attributable to the short duration of the amplifier gain.

These first-generation x-ray laser cavity experiments give us confidence in the viability of multilayer optics and the associated alignment and measurement technologies that are needed for the development of advanced x-ray laser systems with improved efficiency, spatial coherence, and brightness. The likely directions for progress in the near term are many: application to shorter-wavelength lasers, development of unstable resonators for single-mode output from cavities

of large Fresnel number, development of cavity and focusing optics for a high-intensity x-ray laser (>10^{13} W/cm^2; pp. 40–41). These applications will require the development of new cavity optics, and the x-ray gain media may also have to be redesigned to provide sufficient gain duration for multiple amplification passes through the cavity.

High-Resolution X-Ray Microscopy

X-ray microscopy is not a new field. Early work dates back to the 1930s. After World War II, the field enjoyed considerable activity, driven primarily by the potential for applications in microbiology and materials microanalysis. However, the postwar enthusiasm for x-ray microscopy was shortlived. The inadequate x-ray technology of the 1960s—weak sources, crude detectors, and nonexistent optics—could not compete with the rapid developments in high-resolution electron microscopy. Indeed, the contribution of electron microscopy to industry, materials science, and microbiology in the past 20 years has been remarkable.

Nevertheless, it was only a matter of time before medical researchers began to rediscover the potential advantages of x-ray microscopy over optical and electron microscopy. In the late 1970s, a new generation of microbiologists began posing sophisticated questions about the dynamic function of and interactions between cellular and subcellular organisms. They were increasingly dissatisfied with the static structural information inferred from dried, "prepared" specimens viewed under high-vacuum conditions. They needed to be able to observe living specimens in a benign aqueous environment in real time, while maintaining a spatial resolution of ~10 nm. X rays are well suited to these needs; they have wavelengths short enough for high-resolution imaging, they penetrate to greater depths than can electrons, and they produce less damage to the specimen per image. In addition, the wavelength- and Z-dependence of x-ray interactions with matter permit a wider variety of contrast mechanisms than do electron interactions.

The great promise of x-ray imaging for biological subjects has contributed powerfully to the revolution in x-ray technology. By the early 1980s, the brightness of available x-ray sources had increased by four to six orders of magnitude, high-resolution optical components were becoming readily available, and efficient, real-time electronic detection was on the horizon. This produced a "renaissance in x-ray microscopy." Indeed, from 1980 to 1987, the number of working, high-resolution x-ray microscopes in the world increased tenfold, and the activity by microbiologists and medical researchers in these projects increased about fivefold.

High-resolution x-ray microscopy, as it is currently performed, is a sophisticated form of microradiography. The contrast mechanism used is the differential x-ray absorption between the constituent materials of the specimen. For wet, biological structures, typically ~1 μm thick and composed of water and carbon-rich organic molecules, interest centers on the "water window" (2.4–4.4 nm) between the *K* absorption edges of oxygen and carbon. In this wavelength range, water is about ten times more transparent than organic material, providing good sample penetration and image contrast.

Recently, Schmahl, Rudolph, and coworkers at Göttingen University in

(a) Multipass cavity

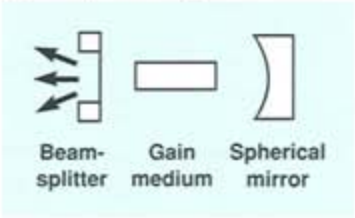

(b) Triple-pass output

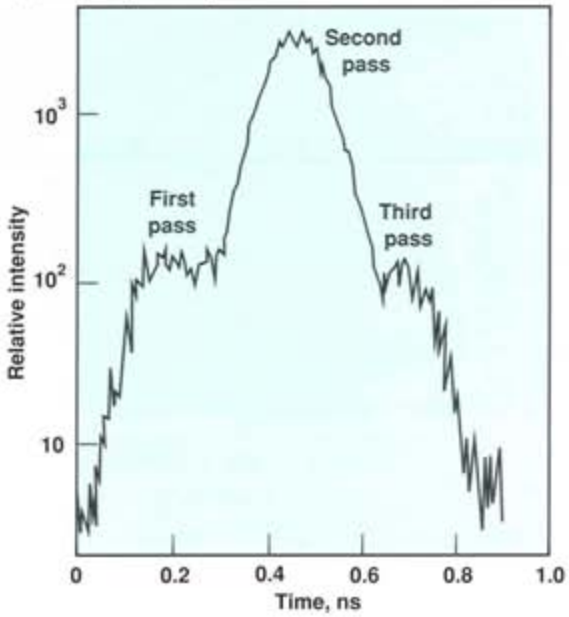

Figure 20. The most sophisticated demonstration to date of soft-x-ray laser cavity performance. Time-resolved, triple-pass amplified output (at 20.63 nm) from a neon-like selenium laser is presented in (b). The reduced amplification of the third-pass beam is due to the short lifetime of the gain medium.

West Germany, have begun to investigate x-ray phase-contrast microscopy, in which the image contrast mechanism is the differential phase modulation in the specimen. X-ray phase-contrast microscopy offers the potential dual advantage of high-contrast imaging at low absorbed dose plus the possible extension to wavelengths outside the water window (e.g., 4.5–5.0 nm) where, although amplitude contrast may be small, phase contrast is large.

Operational, high-resolution x-ray microscopes are of two types: imaging and scanning systems. The imaging microscopes typically use a Fresnel zone-plate condenser lens to concentrate x rays from a synchrotron onto a specimen. The transmitted x rays are collected by a Fresnel zone-plate objective lens, and the magnified image is projected onto a two-dimensional detector array.

Scanning microscopes use a Fresnel zone-plate lens to produce a diffraction-limited, reduced image of an apertured portion of a synchrotron beam. The specimen is scanned across the small x-ray spot, and the transmitted x rays are counted by a high-quantum-efficiency detector and recorded as a function of position. Once the scan is completed, the stored image is processed and reconstructed digitally. Image resolution is limited theoretically only by the diffraction-limited x-ray spot size.

Imaging vs Scanning Microscopy

At present, the imaging microscope technology is somewhat more advanced than its scanning counterpart. However, each approach has its advantages. The main advantage of a scanning system is that, in principle, it can produce an image of given contrast, resolution, and information content (i.e., total number of resolution elements) at a considerably lower dose than can a comparable imaging microscope. This is because all inefficient optics are upstream of the sample, and a simple, high-quantum-efficiency detector can be used, since spatial resolution is not required. Thus, very few of the x rays passing through the specimen are wasted due to inefficiency in the optics or detector. On the other hand, there are many applications where an imaging microscope would be more appropriate. For example, when a lethal or damaging dose is unavoidable, an image can still be

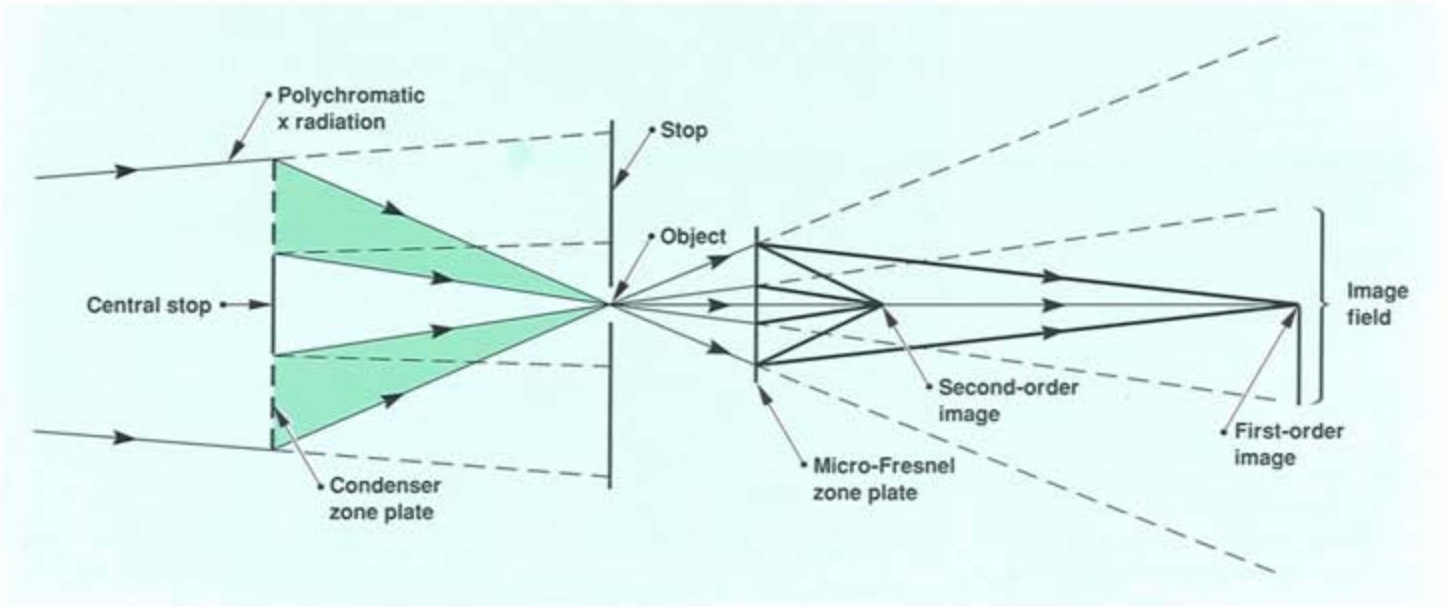

Figure 21. Schematic illustration of the imaging x-ray microscope of Rudolph, Schmahl, and coworkers in Göttingen, West Germany. This device is the most advanced, high-resolution imaging microscope in the world today. It has a demonstrated resolution of approximately 50 nm.

obtained by using a pulsed exposure so short that the image is acquired before the sample is altered.

In the following paragraphs, we briefly describe the most advanced imaging and scanning microscopes in the world today.

Göttingen Group

The imaging microscope of Rudolph, Schmahl, and coworkers is the x-ray analog of an optical microscope in the critical illumination configuration. The optical arrangement is illustrated in Figure 21. An apodized Fresnel zone-plate condenser lens produces a 50× reduced image of the BESSY synchrotron beam onto the specimen (the beam is polychromatic and has a diameter of ~1 mm at its tangent point). A pinhole in the specimen plane (~20 μm diam) defines the field of view while also serving to spectrally filter the beam. The bandpass of this zone-plate pinhole linear monochromator is

$$\Delta\lambda \sim 2d\,(\lambda/D)\,,$$

where D is the condenser zone-plate diameter and d is the pinhole diameter. The condenser zone plate typically used has the following characteristics: $D = 9$ mm, central zone radius $r_1 = 370$ μm, and $d = 20$ μm, producing a bandwidth $\Delta\lambda \sim 0.02$ nm centered about $\lambda = 4.5$ nm (i.e., $\lambda/\Delta\lambda \sim 225$).

The critically illuminated specimen is imaged in transmission by a high-precision micro-Fresnel zone plate with (typically) $r_1 = 1.76$ μm, outermost radius $r_N = 27.8$ μm, $N = 251$, and outermost zone width $\Delta r = 56$ nm. An on-axis field stop is often used to reduce interference from higher-order images. The first-order image spatial resolution of ~50 to 60 nm is magnified ~500× and projected onto photographic film or a microchannel-plate array (or more recently onto a CCD camera).

This sophisticated imaging system has produced a wide array of impressive, high-contrast images of biological specimens with a spatial resolution of ~50 nm. Typical exposure times for such images are on the order of tens of seconds, depending on beam conditions and sample characteristics. Figure 22 shows a phase-contrast image of a dry spore of the Australian moss *Dawsonia superba*. This image required a 40-s exposure time (spore thickness of several micrometers, beam current ~136 mA, x-ray image magnification ~350×). A similar image of a wet *Dawsonia superba* spore required a 30-s exposure (beam current ~220 mA, x-ray image magnification ~250×).

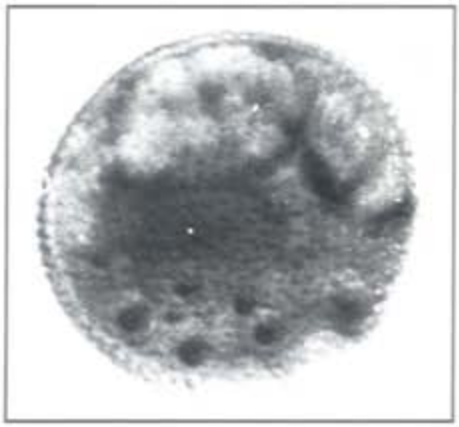

Figure 22. A phase-contrast image of a dry spore of the Australian moss, *Dawsonia superba*, taken with the imaging microscope of Rudolph, Schmahl, and coworkers. Nominal image resolution is ~50 nm.

NSLS Group

The scanning x-ray microscope of Kirz, Rarback, and coworkers operates at a wavelength of 3.2 nm on the undulator beamline at the NSLS, at Brookhaven National Laboratory. The microscope uses the Fresnel zone-plate optical system shown in Figure 23. Emission from the undulator is dispersed by a toroidal grating monochromator ($\lambda/\Delta\lambda \sim 500$) and collimated to provide narrowband, spatially coherent illumination ($dAd\Omega \sim \lambda^2$) of a zone-plate focusing lens. The zone plate is apodized and the focal spot is apertured to eliminate zeroth-order background illumination of the specimen. The zone plate focuses the collimated undulator emission to a diffraction-limited x-ray spot, through which the sample is mechanically scanned.

X rays transmitted through the sample are detected by a flow-proportional counter operated at atmospheric pressure. The proportional counter has no need of spatial resolution. The focusing zone plate currently used in the scanning microscope has a minimum zone width of 70 nm and a total of 205 zones. (Its outer diameter is 57.4 μm, and its focal length at 3.2 nm is 1.3 mm.) A higher-resolution zone plate ($\Delta r = 50$ nm, $N = 311$, $2r_N = 62$ μm, $f = 1.0$ mm at 3.2 nm) will soon be fabricated and installed. This

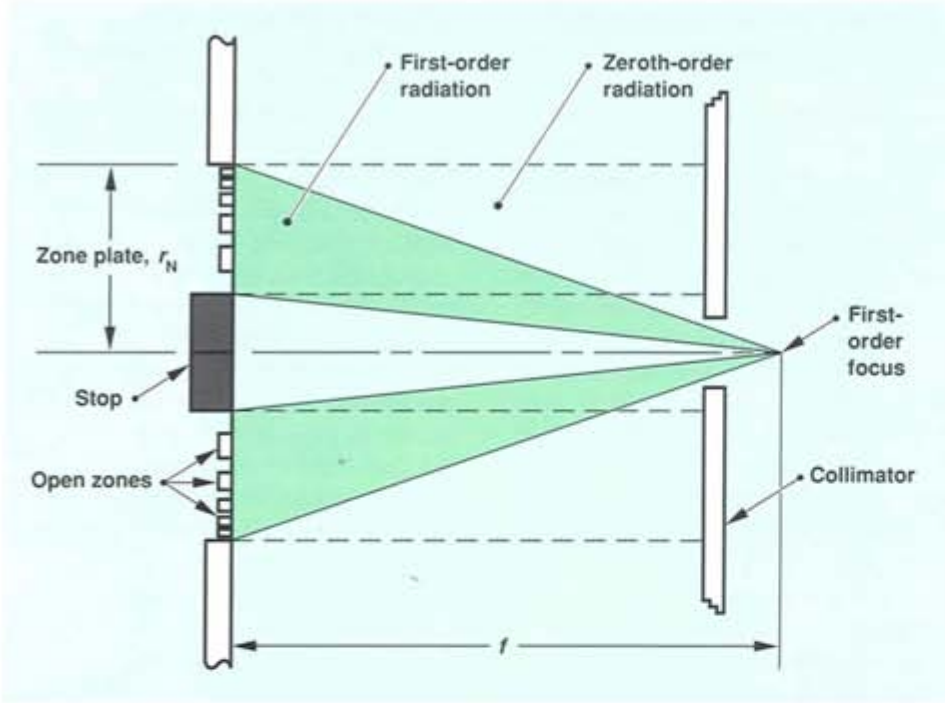

Figure 23. Schematic illustration of the zone-plate focusing geometry of the scanning x-ray microscope of Rarback, Kirz, and coworkers of NSLS. This is the most sophisticated high-resolution scanning microscope currently in operation. It has a demonstrated resolution of ~75 nm.

microscope has demonstrated a spatial resolution of approximately ~75 nm and has produced high-resolution images of wet, unstained zymogen granules. Image acquisition time was on the order of minutes.

X-ray microscopy in the last decade, as typified by the NSLS and Göttigen work, has come a long way. Instruments have performed to design specifications, high-resolution images (~50 to 75 nm) of wet, unstained biological specimens have been produced, and new zone-plate lenses are being developed that will improve spatial resolution to ~10 nm.

Perhaps most important, fruitful collaborations are being established between physicists, who design and build the instruments, and medical researchers, who will lead and apply this technology to important problems in microbiology. The hope is that, through these collaborations, what began as a revolution in technology will lead to a broader and

Figure 24. Schematic illustration of the simple illumination geometry for the Gabor in-line holograms recorded by Howells and coworkers of Lawrence Berkeley Laboratory. (This setup was used to record the high resolution hologram of Figure 25.)

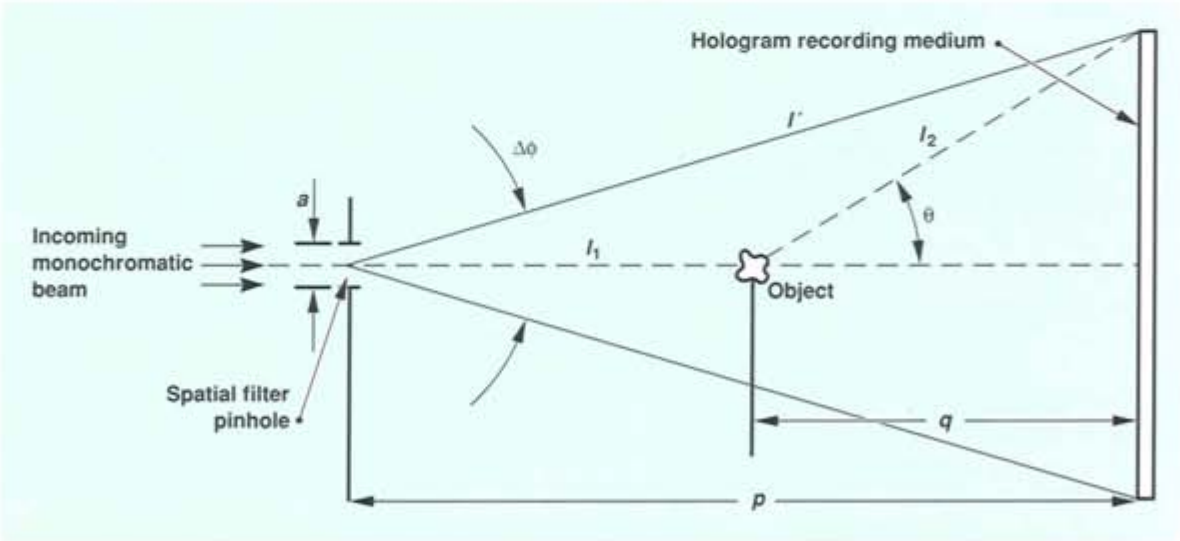

more significant revolution in human health and disease control.

X-Ray Holography

Since Gabor's first proposal in 1947 for holographic microscopy, the possibility of lensless, high-resolution imaging with three-dimensional structural detail has had a great appeal for x-ray microscopists. Work on x-ray holography began in the early 1950s, with the ultimate goal of producing three-dimensional images of cells and other biological structures. Although x-ray holographic investigations continued for three decades, experimental progress was slow and somewhat disappointing until the emergence of high-brightness, coherent x-ray sources in the mid-1980s. In fact, the first demonstration of submicrometer resolution in an x-ray hologram was only recently reported. This was achieved using the first undulator beamline at the NSLS. Almost simultaneously, the first flash hologram, taken in a subnanosecond exposure, was achieved using the selenium x-ray laser at LLNL.

Gabor Geometry

Holography theory and technique have been extensively documented. The simplest holographic configuration is the Gabor in-line geometry, illustrated in Figure 24. It is also the only configuration used with any significant success at x-ray wavelengths. In the Gabor geometry, an incoming x-ray beam is spectrally and spatially filtered to provide temporally and spatially coherent illumination of an object. The hologram records the interference between unscattered reference wavefronts, which pass undiffracted and unabsorbed through and around the object, and scattered wavefronts, which are diffracted from the object's three-dimensional structure.

This interference pattern is recorded as a complex, two-dimensional intensity distribution, or hologram. It contains detailed information about the three-dimensional structure of the object. This structural information may be retrieved later by diffraction of a reference wave replica through the holographic interference pattern. This may be achieved optically or numerically (though not without difficulty).

The great appeal of holography is in the simplicity of hologram recording and the potential for diffraction-limited three-dimensional imaging. That is, given sufficiently coherent illumination and a sufficiently high-resolution detector, the three-dimensional structural information about an object can be simply recorded (i.e., no optics required). In general, the temporal and spatial coherence requirements on the illumination beam are, respectively:

$$\lambda^2/\Delta\lambda > (l_1 + l_2 - l')_{max} ,$$

and

$$\lambda > (a\Delta\phi)/2 ,$$

where $\Delta\lambda$ is the spectral bandwidth, a is the pinhole diameter, $\Delta\phi$ is the divergence of the spatially filtered beam, and $(l_1 + l_2 - l')_{max}$ represents the maximum optical path difference between the scattered and reference waves (see Figure 24). The diffraction-limited lateral (δ) and longitudinal (Δ) resolution are given by

$$\delta \sim \lambda/\theta ,$$

and

$$\Delta \sim \lambda/(2\theta^2) ,$$

where θ is the maximum collection half-angle of scattered radiation recorded in the hologram. Resolution can be compromised by blurring of the hologram due to finite pinhole size and/or limited detector resolution. In this regard, diffraction-limited resolution requires a pinhole size a

$$a < (p/q)\ \lambda/\theta ,$$

and a detector resolution G of

$$G < (1 - q/p)^{-1}\ \lambda/\theta .$$

In addition, background interference can be minimized in the reconstructed image if the hologram is recorded in the far field, i.e.,

$$w << (\lambda q)^{1/2} ,$$

where w is the lateral dimension of the object.[2]

The highest resolution in x-ray holography to date was demonstrated by Howells and colleagues, of the Lawrence Berkeley Laboratory, working on the X17t undulator beamline at the NSLS. In these experiments, the undulator beam was spectrally filtered by a toroidal grating monochromator with a resolving power of $\lambda/\Delta\lambda \sim 700$, providing a coherence length ($\lambda^2/\Delta\lambda$) of ~ 1.8 μm at 2.47 nm. The beam

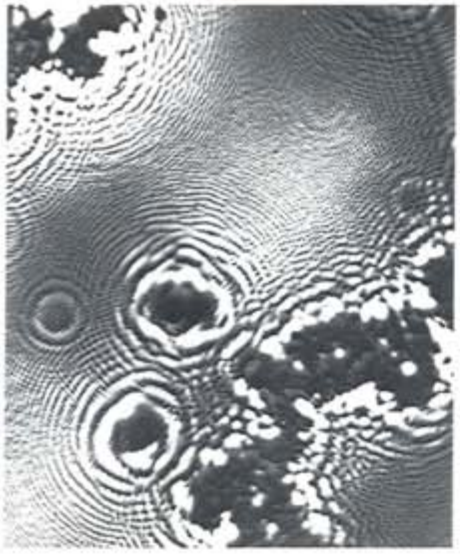

Figure 25. The highest resolution x-ray hologram recorded to date. The holographic image, recorded by Howells and coworkers, is of several zymogen granules. Structural information on a 40-nm scale has been recorded. The overall dimensions of the figure shown are 19 μm × 15 μm.

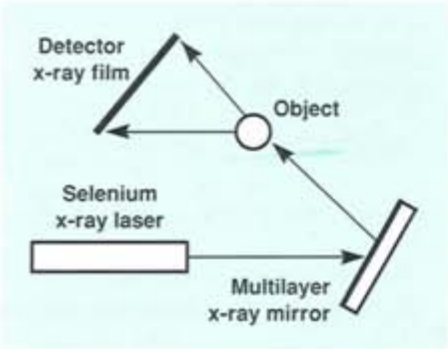

Figure 26. Schematic illustration of the simple illumination geometry for the Gabor in-line holograms recorded by Trebes and coworkers at LLNL. The setup was used to record the first x-ray flash (~200-ps) holograms and the first x-ray holograms utilizing an x-ray laser source.

was spatially filtered by a 50-μm-diam pinhole located 1.74 m upstream of the sample. This provided coherent illumination (in the Gabor geometry) over a ~61-μm-diam circular area at the sample plane. The coherent photon fluence was on the order of 10^8 photons/s at 2.47 nm. The samples were dried zymogen granules from a rat pancreas. A TEM image of the recorded hologram is shown in Figure 25. The hologram recording time was 80 min, representing an exposure of $\sim 8 \times 10^{11}$ photons ($\sim 6 \times 10^{-5}$ J), or an absorbed specimen dose of 2×10^8 rad (1 rad = 10^{-5} J/g absorbed dose). The hologram was recorded in a 200-nm-thick resist film located approximately 400 μm downstream of the sample. From the measured hologram fringe frequency, the transverse resolution is estimated to be ~40 nm.[3] Numerical reconstruction of the hologram has been carried out. The initial results appear to verify the presence of structural information on a 40-nm spatial scale, although the quality of the reconstructed image is insufficient to provide significant new insight into zymogen granule structure.

Flash Hologram Demonstration at LLNL

Another interesting demonstration of x-ray holography was recently performed by Trebes and colleagues at LLNL using the selenium x-ray laser source. In these experiments, the Gabor in-line geometry was also used (see Figure 26). The direct output of a 4-cm-long selenium x-ray laser was reflected off a multilayer mirror and onto the object. No additional spatial filtering was employed. In this set-up, the x-ray laser emission was estimated to be ~500 kW, at 20.63 and 20.96 nm, in a short pulse of about 200 ps FWHM. The multilayer mirror had a 10% bandwidth and was used to reduce the background continuum radiation from the hot laser plasma. A thin aluminum filter foil was used to protect the holographic film from visible and ultraviolet light. The laser-to-object distance was 3.65 m, the object-to-hologram distance was 5.08 cm, and the recording medium was an x-ray film with a resolution of ~5 μm.

A typical specimen was an 8-μm-diam carbon fiber. The recorded holographic interference pattern from such a fiber is shown in Figure 27. Since the structure of the object is fairly simple, the hologram fringes can be easily calculated (an x-ray laser source diameter of ~70 μm is assumed). The calculated fringes are also shown in Figure 27. The good agreement between the measured and calculated fringe patterns is testament to the high degree of control exercised over the source and exposure parameters. Optical reconstruction of the x-ray holograms was performed using a helium-neon laser at 632.8 nm. As in other demonstrations, the reconstructed images verified the anticipated hologram resolution (~5 μm in this case, limited by film resolution) without producing a high-quality image of the object.

The LLNL holography demonstration used a detector approximately a million times more sensitive and achieved a spatial resolution about 100 times worse than the NSLS experiment. In this

(a) Fringe pattern

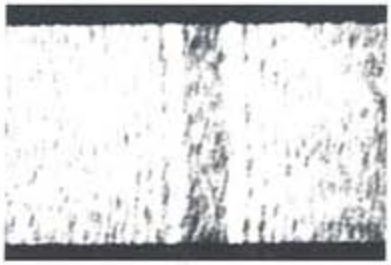

(b) Measured x-ray intensity

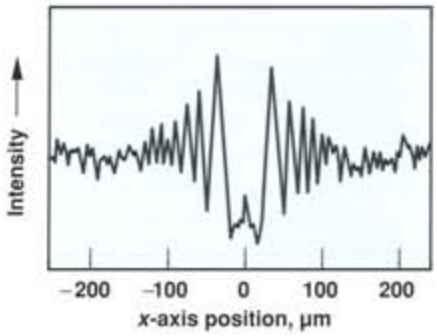

(c) Calculated x-ray intensity

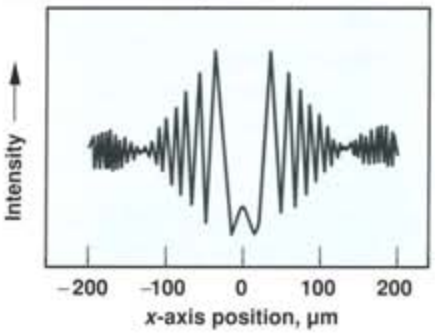

Figure 27. X-ray holography data taken by Trebes and coworkers (see Figure 26). Holographic interference patterns from an 8-μm-diam carbon fiber are shown. (a) Fringe pattern on film; (b) measured linear fringe intensity; (c) calculated linear fringe intensity.

regard, it is not particularly relevant to the problem of holographic microscopy of biological samples. However, in a broader sense, it is an eloquent statement of how far the technology for x-ray holography has progressed. It is remarkable that good-quality, single-shot, flash holograms (~200-ps time scale) of tiny objects (~5–10-μm scale) are being produced quite simply by illuminating the specimen with an x-ray laser beam. The technology is reminiscent of the state of optical holography in the mid-1960s.

Holography in Perspective

As a competitive technique for ultrahigh-resolution microscopy, holography suffers from a number of disadvantages that offset the simplicity of hologram recording. The requirement of coherent illumination demands sources of very high spectral radiance. The high information content of a quality hologram (i.e., high signal-to-noise ratio) requires high-resolution detection and a very high count rate, leading to specimen dose problems.[4] In addition, holography requires image reconstruction. Optical reconstruction is impractical for ultrahigh-resolution work. Numerical reconstruction, on the other hand, will require sophisticated STEM and densitometry to extract high-resolution exposure information from resist profiles as well as detailed models of nonlinear resist recording mechanisms to produce quantitative, aberration-free images. There are also fundamental questions about the limits on information retrieval that can be achieved in holographic imaging at the diffraction limit.

Nevertheless, the value of x-ray holography should not be judged solely on the basis of its viability for the near-term microscopy of biological samples.[5] Holography is a complex technology with its own unique set of challenges and capabilities, and the prospects for x-ray holographic imaging have never been more promising. New undulator and x-ray laser sources will soon be available with spectral radiance values two to four orders of magnitude higher than current sources. They will allow the achievement of much higher signal-to-noise ratios in x-ray holograms; they will also make possible the use of off-axis and Fourier-transform geometries to alleviate some of the problems associated with image reconstruction and high-resolution detection. The achievement of significantly higher signal-to-noise ratios will also permit a better assessment of the fundamental limits on holographic imaging and a better definition of the role of holography in the cast of new x-ray capabilities.